

# FLAG-SHAPED BEHAVIOR DAMPER USING THE COMBINATION OF FRICTION AND RUBBER SPRINGS

Eunsoo Choi<sup>\*1</sup>, Gyuchan Choi<sup>\*2</sup>, Joowoo Kim<sup>\*3</sup>, Kyoung-Taek Yang<sup>\*4</sup>

<sup>1,2</sup>Department of Civil Engineering, Hongik University, Seoul, Korea  
[eunsoochoi@hongik.ac.kr](mailto:eunsoochoi@hongik.ac.kr) / [chirbcks@naver.com](mailto:chirbcks@naver.com)

<sup>3</sup>Department of Architectural Engineering, Semyung University, Jechung, Korea  
[jw\\_kim@semyung.ac.kr](mailto:jw_kim@semyung.ac.kr)

<sup>4</sup>Department of Mechatronics Engineering, Dalim College, Ahnyang, Korea  
[ktyang@daelim.ac.kr](mailto:ktyang@daelim.ac.kr)

**Key words:** Friction, Rigid-elastic behavior, Smart damper, Flag-shaped, Recentering

**Summary:** *This study proposes a new concept of a smart damper to provide flag-shaped behavior using the combination of magnetic friction and rubber springs. The magnet provides energy dissipation due to friction, and the rubber springs with precompression contribute to increasing the recentering capacity of the damper. To verify their performance, dynamic tests of magnet frictional dampers and precompressed rubber springs were conducted. For this purpose, hexahedron neodymium (NdFeB) magnets and polyurethane rubber cylinders were used. In the dynamic tests, the loading frequency was varied from 0.1 to 2.0 Hz. The magnets showed almost perfect rectangular behavior in the force-deformation curves, and the frictional coefficient of the magnets was estimated through averaging and regression. The rubber springs were tested with and without precompression. The rubber springs showed different loading path from the second cycle and residual deformation that was not recovered immediately. The precompressed rubber spring showed rigid-elastic behavior with hysteresis in the elastic region. The rubber springs showed greater rigid force with increasing precompression. Finally, this paper discusses the combination of rigid-elastic behavior and friction to generate 'flag-shaped' behavior for a smart damper and suggests how to combine magnets and rubber springs to obtain flag-shaped behavior. The performance of the magnets and precompressed rubber springs was verified through analytical models.*

## 1 INTRODUCTION

Dampers are used to dissipate input energy and reduce vibration of a system; thus, they are used in various fields. In civil engineering, they are mainly applied in the protection of bridges and buildings from seismic attacks [1]. In addition, they are used to control the vibration of structures induced by vehicles [2], human beings [3], or environmental loadings [4]. There are several types of dampers, including fluid dampers, frictional dampers, and metallic dampers. The first type includes viscous, magnetorheological (MR) [5], [6], [7] and electrorheological (ER) dampers [8]; they use a special fluid to dissipate input energy. These

dampers cannot avoid the problems of aging and fluid leaking; thus, this increases the cost of maintenance for replacing the fluid. Conventional frictional dampers generally use mechanical friction provided by bolt tensions [9]. In these dampers, slight variation of bolt-tension or the surface-condition of frictional material may reduce frictional force. These types of dampers provide excellent energy dissipation capacity; however, they do not provide recentering (or self-centering) capacity. Thus, structures or systems that incorporate them could be dislocated from the as-built location after an earthquake. To overcome this problem, smart dampers with a flag-shaped behavior have been introduced [10],[11].

Dolce et al. (2000) proposed a smart damper using shape memory alloy (SMA) wires. They used martensitic and superelastic SMA wire to provide energy dissipation and recentering capacity, respectively. This damper successfully provides the flag-shaped behavior and recovers the displacement of structures without any dislocation. However, NiTi SMAs used in the Dolce's study are very expensive in comparison with steel, and the components and design of the SMA damper are complicated. After Dolce's study, several variations of smart dampers using mechanical friction and springs have been suggested, and they basically used the combination of energy dissipation and recentering group to realize smart behavior [12].

There are two types of dampers depending on whether or not there is contacting between magnets and magnetic substances; that is contacting or non-contacting. In the non-contacting case, a conductor moves in a magnetic field and a magnetic drag force is generated. A specific type of damper using this principle is an eddy current damper [13],[14] mentioned that the eddy current damper has several advantages compared with other types of dampers; they have no mechanical contact and show high reliability, easy tuning capacity, and high thermal stability. However, the critical disadvantage of the eddy current damper is its relatively small damping force. Several studies of eddy current dampers have been conducted for the applications of structures. However, the provided damping forces in the studies were not strong enough for real structures. The damping ratio or damping force of an eddy current damper decreases exponentially with increasing distance between the magnet and conductor. Thus, to increase the damping force, the distance should be minimized. The extremity of minimization is contact; in other words, no gap between the magnet and conductor. In this case, frictional force develops between the magnet and conductor. [15] introduced a ball-screw-type magnetic friction damper to generate damping force, and they obtained the typical frictional behavior of rectangular-shaped behavior. [16] suggested another type of magnetic friction damper using a rack and rare-earth magnets. This type of damper has a long stroke; however, frictional force depends on the vibrational frequency, and its behavior shape is not rectangular. In these two types of magnetic friction dampers, the friction is generated during the rotation of the magnets.

In this paper, a new concept of smart damper will be proposed that using the friction of permanent magnets and pre-compressed rubber springs; the magnetic friction provides energy dissipation capacity and the pre-compressed rubber springs provide recentering capacity. For this purpose, a series of dynamic tests of magnetic friction dampers and pre-compressed rubber springs were conducted. The smart damper will be explained by analytical models based on the experimental results of the two components.

## **2 DYNAMIC TESTS OF MAGNETIC FRICTION DAMPER**

### **2.1 Magnetic friction damper**

In this study, hexahedron neodymium (NdFeB) magnets with dimension of 50 mm x 50 mm x 25 mm (BxLxH) were used to provide magnetic friction (see Figure 1).



Figure 1 : Shape of the magnet

To estimate the adhesive strength of the magnet due to magnetic force, a simple tensile test was conducted as shown in Figure 2.



Figure 2 : Tensile test of the magnet

The magnet was placed between two steel plates; on the upper plate, a load-cell was connected to measure tensile force. The average ultimate magnetic force of the magnet was measured as 0.8 kN; this force works as a normal force of friction.

The magnetic friction damper developed in this study consists of two rectangular inner and outer tubes (see Figure 3).

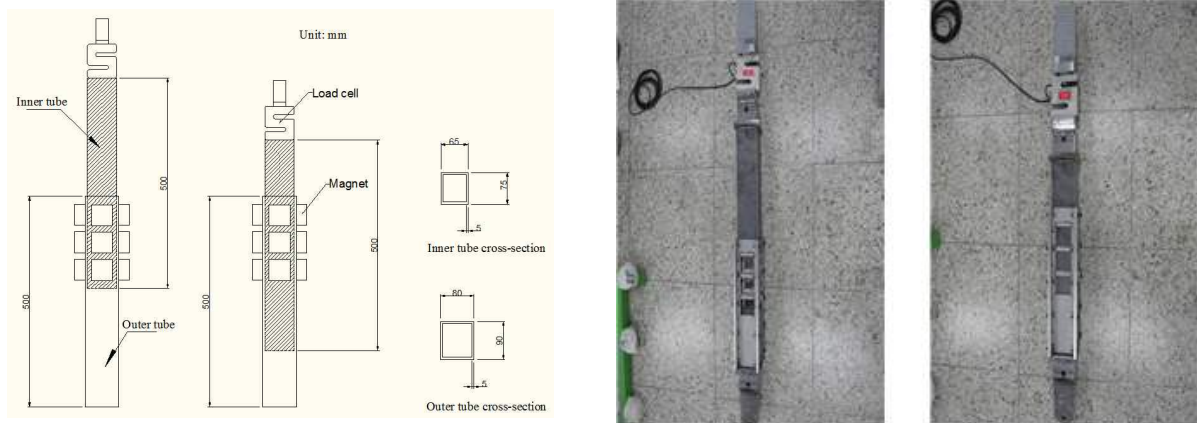


Figure 3 : Shape of the magnetic friction damper in pull-out and push-in position

The length of both tubes is 500 mm, and the thickness of the side plates is 5 mm. The outer dimensions of the inner tube are 65 mm x 75 mm (BxL), and the corresponding values of the outer tube are 80 mm x 90 mm. The inner one slides inward and outward through the outer one. The inner one is made of steel; thus, the magnet can be attached on the plate of the tube. However, the material of the outer tube is aluminum, which is a non-magnetic substance. The outer tube has three square holes in each side of the plate with dimensions of

51 mm x 51 mm (BxL); thus, a total of 12 holes are placed in the outer tube. The length of each side of the hole is larger by 1 mm than the width of the magnet. Each magnet is attached on the inner tube through the holes in the outer tube. When the inner tube is moving, the movement of the magnets is restricted by the outer tube; thus, sliding between the magnet and inner tube occurs, and friction accompanies by the sliding. A load-cell was mounted on the top of the inner tube to measure the pushing and pulling force of the damper.

## 2.2 Dynamic tests

Dynamic tests were performed based on the two parameters of loading frequency and number of magnets. The number of magnets represents the variation of normal force of friction, and it was varied from 2 to 12 with an increment of 2. This means that the minimum normal force was 1.6 kN, and the force increased to 9.6 kN with an increment of 1.6 kN. The loading frequencies were 0.1, 0.25, 0.50, 0.75, 1.0, and 2.0 Hz; the loading with 0.1 Hz represents quasi-static loading. The loading frequency was varied to investigate the sensitivity of the damper to vibrational frequency. Most civil structures such as bridges and buildings have a fundamental natural period in lateral vibration with a range of 0.5 to 1.0 sec. If they are equipped with isolation devices from ground motions, their lateral fundamental periods become longer while they may not exceed 5 sec. Thus, in the dynamic test, the minimum and maximum loading frequencies can be 0.2 and 2.0 Hz, respectively. The loading frequency of 0.1 Hz was assumed to be quasi-static case. Five cycles were loaded for each frequency. Based on the performance of the dynamic UTM (Universal Test Machine), the strokes were varied according to loading frequency;  $\pm 10$  mm for 0.1-0.5 Hz,  $\pm 5$  mm for 0.75-1.0 Hz, and  $\pm 2$  mm for 2.0 Hz. In the test set-up (see Figure 4), a displacement transducer was mounted on the top of the inner tube to measure the translational movement of the damper.

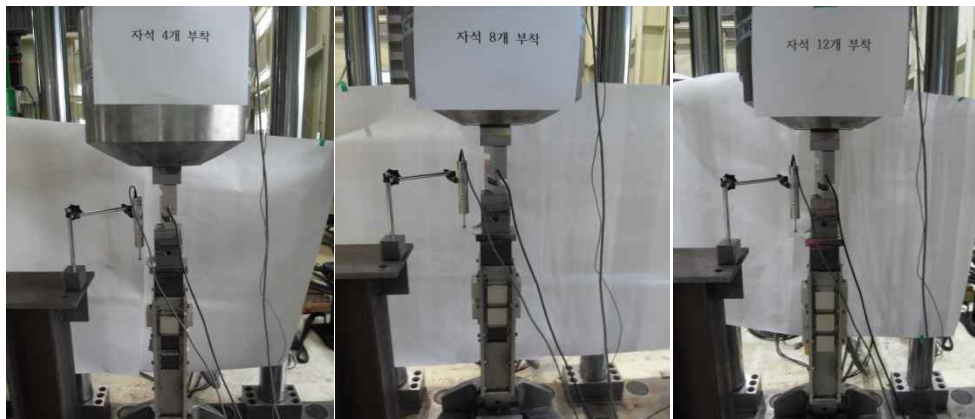
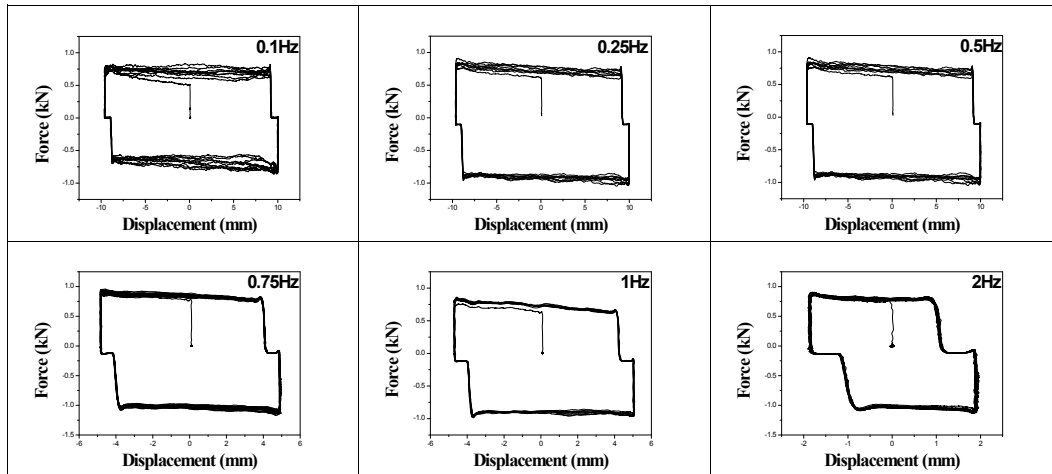
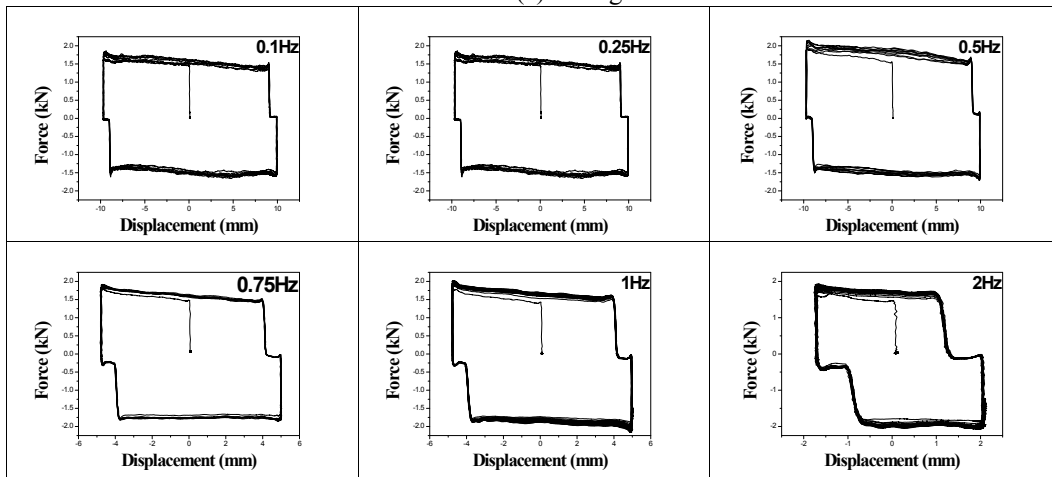


Figure 4 : Test set-up and shape of damper with the magnets

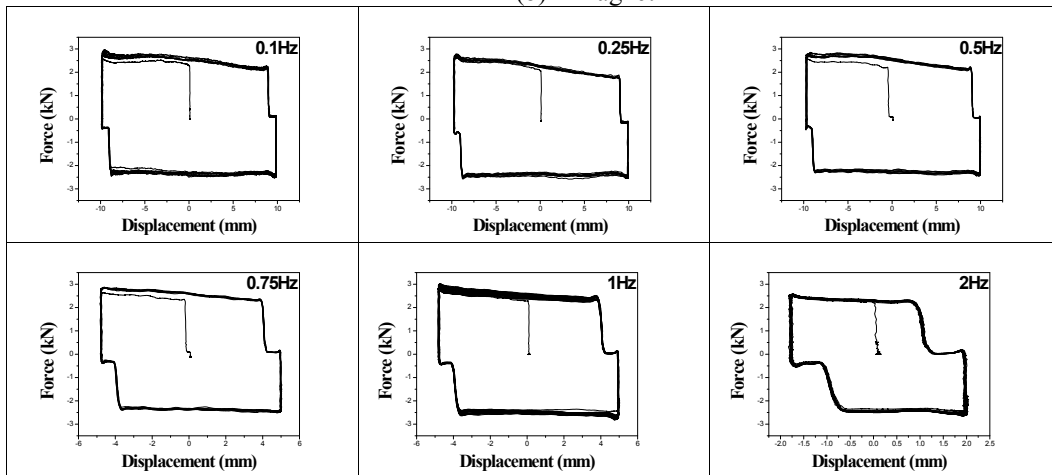
The force-displacement curves of the magnetic friction damper are shown in Figure 5, where positive displacement represents pushing in and negative value does pulling out.



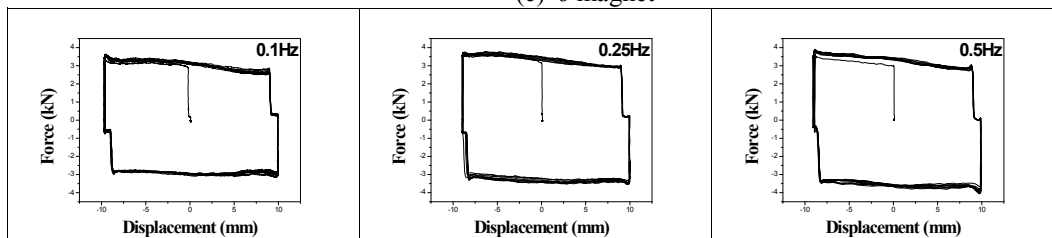
(a) 2 magnet

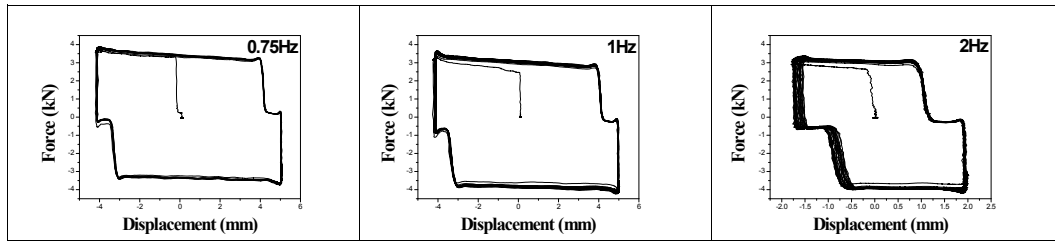


(b) 4 magnet

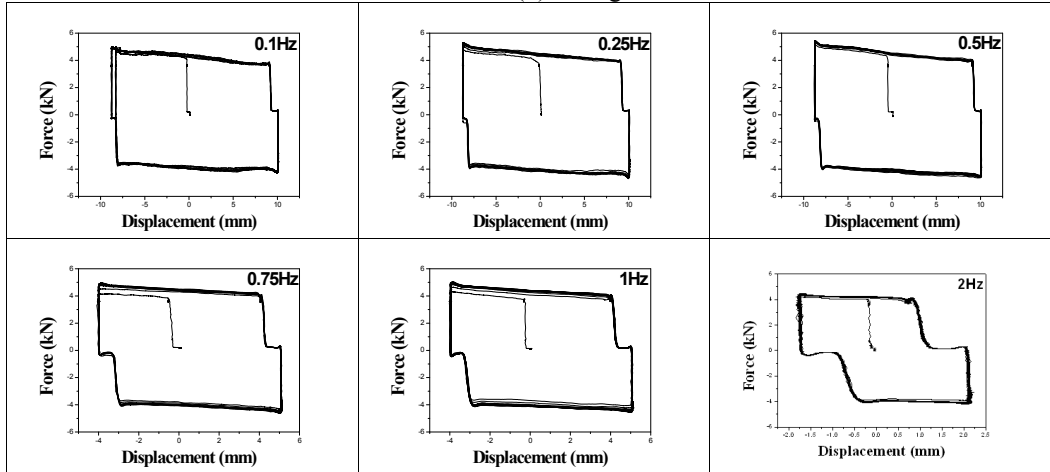


(c) 6 magnet

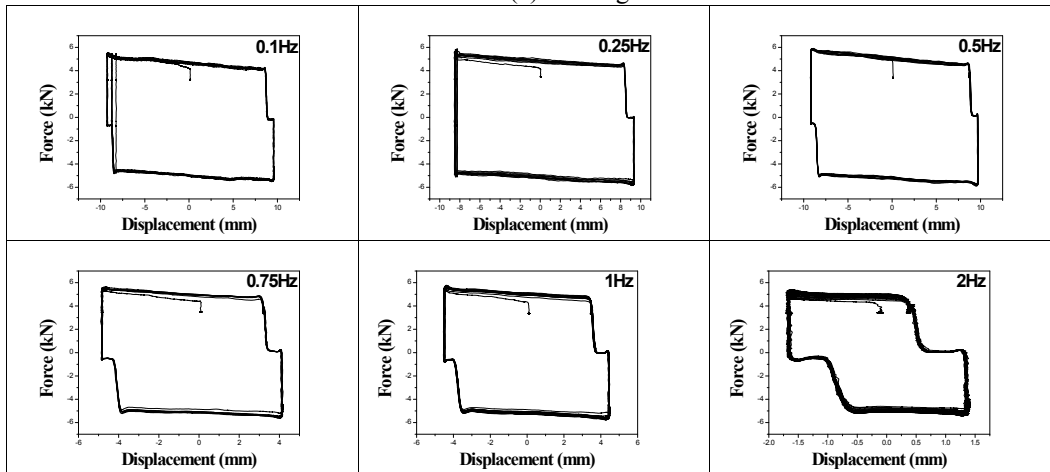




(d) 8 magnet



(e) 10 magnet



(f) 12 magnet

Figure 5 : Force-displacement curves of the magnetic friction dampers

As seen in Figure 5(a), for the first three tests of 0.1, 0.25, and 0.5 Hz, bands of frictional forces are observed. Then, the band-magnitude decreases with subsequent tests. It appears that the band was caused by the irregularity of the surface of the inner tube, on which the magnets slide. In the curves, a step is observed with the reversing stroke since there is a gap of 1.0 mm between the magnets and holes in the outer tube. The last observation is that there is a slope on the upper frictional lines, which are on pull-out phase. This was caused by the developed inertia force of the inner tube. This inertia force increases with increasing moving speed. The maximum moving speed of the damper is 20 mm/sec for the cases of 0.5 and 1.0 Hz vibration. Thus, the slopes of the two cases are larger than those of the other cases. This influence of the inertia force will disappear if the damper is installed horizontally.

### 2.3 Frictional force and coefficient

The frictional force of the damper is estimated as the average of the forces crossing the y-axis in the force-displacement curves. In Figure 6, the variation of magnetic friction is shown according to frequency.

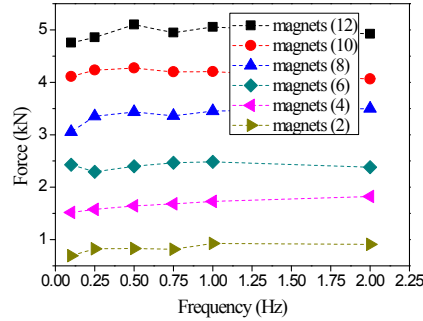


Figure 6 : Magnetic frictional force as a function of frequency

The frictional coefficient  $\mu$  can be obtained from the estimated frictional forces using the following equation:

$$F = \mu N \tag{1}$$

where  $N$  is the normal force induced by magnetic force and  $F$  is the frictional force. The normal force can be obtained by multiplying the number of magnets by 0.8 kN which is the ultimate magnetic force of the magnet. The estimated frictional coefficients are shown in Table 1.

No. Of Magnets	Frequency (Hz)					
	0.1	0.25	0.5	0.75	1.0	2.0
2	0.431	0.519	0.519	0.513	0.581	0.569
4	0.472	0.494	0.513	0.525	0.541	0.569
6	0.506	0.477	0.500	0.513	0.517	0.496
8	0.477	0.523	0.538	0.523	0.539	0.547
10	0.513	0.529	0.534	0.525	0.525	0.508
12	0.495	0.506	0.531	0.516	0.526	0.513
Average	0.482	0.508	0.522	0.519	0.538	0.533
Regression	0.496	0.512	0.529	0.520	0.528	0.519

Table 1 : Frictional coefficients of the magnetic friction damper

Figure 7 shows the average frictional coefficient as a function of frequency. The frictional coefficient increases until the frequency of 0.5 Hz; after that, it becomes stable. It appears that the relatively small value of 0.75 Hz is an experimental deviation. Figure 7 shows another estimated frictional coefficient using a linear regression between the normal and

frictional force. In Figure 6, the slopes of the regression represent the frictional coefficient. In the graphs in Figure 6, the x-axis is the number of magnets, which can be converted to the normal force by multiplying 0.8 kN. Thus, the frictional coefficient can be obtained by the slopes divided by 0.8. The result is shown in Table 1 and compared with the average frictional coefficient in Figure 7.

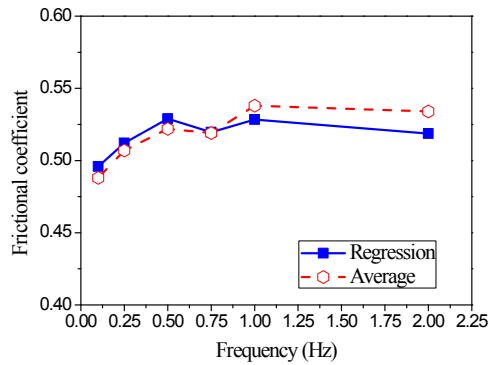


Figure 7 : Frictional coefficients from average and regression

The result of the regression shows relatively larger coefficients than the values from average with low frequencies under 0.5 Hz. However, in the high frequencies above 1.0 Hz, the trend is reversed. Based on the regression, the frictional coefficient increased sharply up to 0.5 Hz and then decreased smoothly until 2.0 Hz. It seems that the result of the regression is more reliable since the regression can straighten the measuring deviation. Therefore, the static frictional coefficient of the magnetic friction is assumed to be 0.496 of 0.1 Hz loading, which was assumed as quasi-static condition. The average value for other cases is 0.522, which is the kinetic frictional coefficient of the magnetic friction.

### 3 PRECOMPRESSED RUBBER SPRING

#### 3.1 Material and test set-up

This study used a rubber cylinder with an inner hole at the center, and its dimensions are shown in Figure 8.

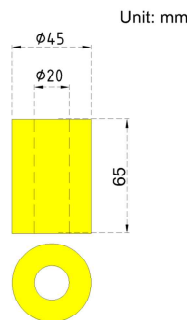


Figure 8 : Shape and dimension of the rubber cylinder

The cylinder is made of polyurethane rubber, whose durometer hardness is 95A, which is much higher than that of natural rubber [17]; the range of durometer hardness for natural rubber varies from 50A to 70A. In general, higher hardness rubber shows a higher Young's modulus. Thus, polyurethane rubber can be used to make a stiffer spring than natural rubber if they have the same shape and dimension. In addition, polyurethane rubber has much higher



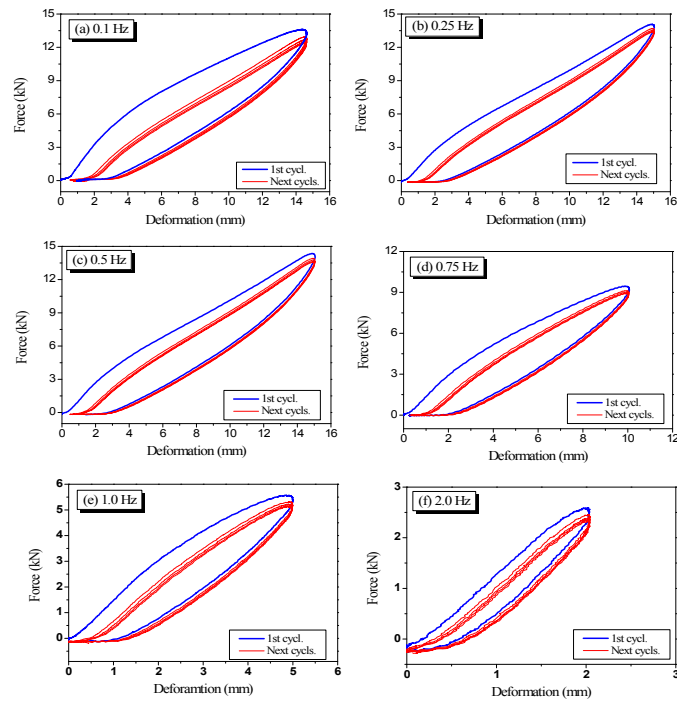


Figure 10 : Cyclic force-deformation curves of rubber springs without precompression

In the first loop in Figure 10(a), there is a gap of 0.5 mm initially. This was caused by imperfect contact between the steel plate and the rubber spring; therefore, this gap should be removed from the behavior of the rubber spring. Thus, the compressive deformation of the rubber spring in the first loop was 14.1 mm, which corresponds to a strain of 21.7%. In the unloading path, the rubber spring did not recover all compressive deformation and there was a residual deformation of 2.5 mm. Before the second reloading, the deformation of 1.0 mm was recovered during the unloading. However, the other deformation of 1.5 mm, which is 2.3% strain, was not recovered during the test; it would take a time to recover this deformation, which acts like a gap for the next cycles from the second one. Thus, the second loading path began from the deformation of 1.5 mm, and the unloading path touched the deformation of 2.5 mm. Because of this, the maximum force of the cycles after the first one at a given deformation became smaller than that of the first cycle. The residual deformation of 1.2 mm for the second cycle was almost recovered during the unloading. However, continuous softening behavior occurred a little at a time after the second cycle. For the dynamic loadings of 0.25 and 0.5 Hz, the residual deformations of the first cycles were 2.5 mm, respectively, which is equal to that of the quasi-static loading. In addition, the recovered deformation and deformation-set of the first cycle unloading for both tests were 1.0 and 1.5 mm, respectively. Thus, it appears that the dynamic loading tests did not change the residual deformation, recovered deformation, and deformation-set, although their loading paths differed from that of the quasi-static test.

### 3.2.2 Damping effect

The rubber spring showed hysteretic behavior for a cyclic loading, and the energy dissipation due to hysteresis helped increase the energy-dissipation capacity of the damper.

Thus, the equivalent damping ratios for the first and next hysteresis of the rubber springs are calculated using the following equation [18]:

$$\xi = \frac{1}{4\pi} \frac{E_D}{E_E} \quad (1)$$

where  $E_D$  and  $E_E$  are the dissipated and elastic energy for a hysteresis.

Table 2 shows the damping ratios for the first cycle of the springs according to the loading frequency compared with those of the second cycle.

Frequency	Non-precompression		Precompression of 5 mm		Precompression of 10 mm	
	1 <sup>st</sup> cycl.	2 <sup>nd</sup> cycl.	1 <sup>st</sup> cycl.	2 <sup>nd</sup> cycl.	1 <sup>st</sup> cycl.	2 <sup>nd</sup> cycl.
0.1 Hz	4.72%	2.80%	3.33%	2.29%	1.90%	1.36%
0.25 Hz	3.67%	2.72%	3.41%	2.53%	1.90%	1.50%
0.5 Hz	3.79%	2.82%	3.38%	2.66%	2.11%	1.67%
0.75 Hz	4.44%	3.22%	3.47%	2.70%	2.28%	1.81%
1.0 Hz	4.68%	3.43%	3.67%	2.73%	2.29%	1.81%
2.0 Hz	3.51%	2.86%	2.50%	2.07%	1.60%	1.32%

Table 2 : Damping ratios of the rubber springs

For the first three frequencies of 0.1, 0.25, and 0.5 Hz, which have the same amplitude, the quasi-static loading case showed a relatively large damping ratio in the first cycle compared to the other two dynamic loading cases. However, for the second cycle, they showed almost the same damping ratio. Thus, it appears that the rubber spring showed a stable damping ratio from the second cycle, even with dynamic loading. For the next three high loading frequencies, the damping ratios increased in comparison with those for the first two dynamic loading frequencies. This was caused by the small amplitudes of the three high frequency cases. For the rubber spring, all damping ratios were smaller than 5% and much smaller than that of the magnetic friction of 63.6%. Thus, the damping of the rubber spring did not have significant influence on dissipating energy in the system. In addition, the damping ratios for the second cycles were too small to significantly reduce the vibration.

### 3.3 Dynamic tests of rubber springs with precompression

#### 3.3.1 Effect of precompression

The typical cyclic behavior of the rubber spring is shown schematically in Figure 11. As mentioned previously, the residual deformation after the first cycle is recovered partially, and the other residual deformation is a set of deformation for the next cycles. For the rubber spring, there are three possible cases of precompression.

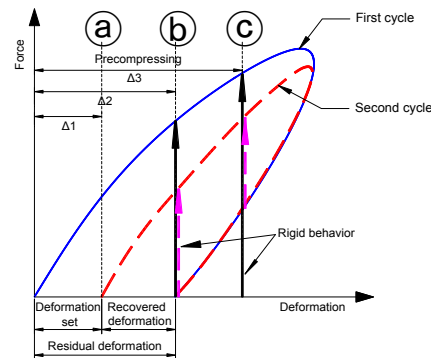


Figure 11 : Effect of precompression in the rubber spring

First, when the amount of precompression is smaller than the deformation set  $\Delta_1$ , the second cycle begins with a gap because of the set. In this case, the hysteretic behavior of the rubber spring is similar to that of an uncompressed one. In the second case, the precompression is located between deformation  $\Delta_1$  and  $\Delta_2$ . In this case, the deformation set is removed by the precompression. Thus, the hysteretic behavior begins without any gap and shows a rigid behavior from the base to the first or second loading path. In the third case, the precompression exceeds the residual deformation  $\Delta_2$  such as the case of © in the figure, and the behavior shows a rigid behavior up to the first loading path. Then, the unloading stops with the remaining force, and the curve goes up to the second loading path rigidly. Then, the curve follows the second loading path. Therefore, in this case, the hysteretic curves do not touch the base of zero force. The most desirable case among the three is the third one; the case of © in Figure 11. The remaining force in this case can be used to increase the recentering or self-centering capacity of the damper.

### 3.3.2 Cyclic behavior under precompression

Two tests were conducted with variation of precompression to 5 and 10 mm. The strokes for the tests and the precompression were controlled to be equal to the strokes of the corresponding non-compression tests. For example, the stroke for the 0.1 Hz test with 5 mm precompression was 10 mm; thus, the summation of 5 and 10 mm became 15 mm. The stroke for the 0.1 Hz with 10 mm precompression was 5 mm; thus, the total became 15 mm. The hysteretic behavior of the precompressed rubber springs was rigid initially. Then, hardening behavior was caused by the additional compression (see Figures 12).

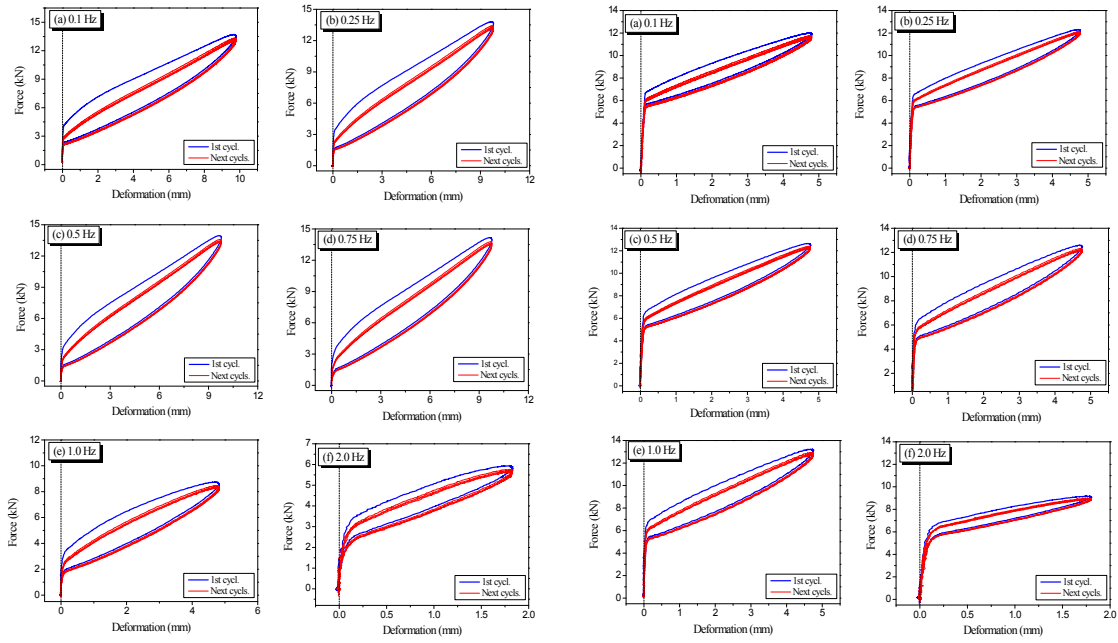


Figure 12. Hysteretic curves of rubber springs with precompression 5mm and 10mm

The hysteretic loops were stabilized from the second cycle. However, the rigid force decreased after the first cycle. This was caused by the residual deformation explained above. The rigid force for the second cycle recovered because of deformation recovery. However, the rigid force of the second cycle is smaller than that of the first cycle because of the deformation set described in the previous section. Therefore, the rubber spring can return to the original location using the precompressing technique. The precompressed rubber springs showed typical flag-shaped behavior, which is usually observed in smart materials, such as shape memory alloys. In flag-shaped behavior, the first rigid behavior assists the recentring capacity of damper, and the hysteresis on the rigid part provides additional damping.

For the case of 5 mm precompression, the initial rigid force is reduced approximately by 50% after unloading of the first cycle. The rigid force for the second loading path is 66% of the first rigid force of the loading path. For the case of 10 mm precompression, the corresponding values are 83% and 89%, respectively. Based on the above result, it appears that the reduction ratio of the rigid force due to the hysteresis is reduced with an increasing amount of precompression. The second cycle behavior should be used for a conservative design.

The effective stiffnesses of the loading hysteretic loops for the first and second cycles were estimated (see Figure 13). In the figure, the subscripts of 1 and 2 represent the first and second cycle, and the second subscripts represent the amount of precompression. The stiffness was estimated as the slopes from the rigid force at the origin to the end point of the loop. For the uncompressive case, the stiffnesses of the first cycle for the first four loading frequencies were stable as 0.97 kN/mm. For the loading frequencies of 1.0 and 2.0 Hz, the stiffnesses increased to 1.15 and 1.39 kN/mm, respectively.

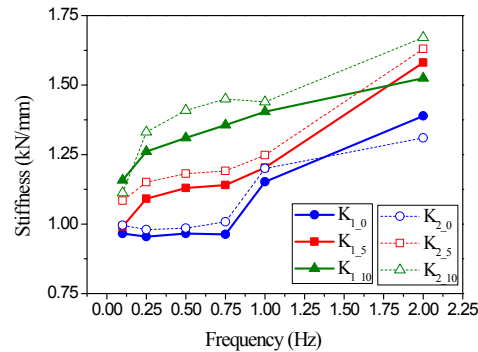


Figure 13 : Effective stiffness of loading paths for the precompressed rubber springs

The strokes of the two cases were shorter than those of the other cases; this produced relatively high effective stiffness. The rubber springs showed stiff behavior at first and then softening behavior. Thus, the effective stiffness increased with a relatively small stroke. The results indicate that the loading effective stiffness of the rubber spring without precompression does not vary according to loading frequency. However, for the precompressed rubber springs, the loading stiffness increased with high loading frequency. The increment ratio of stiffness for the 10 mm precompression case was larger than that for the 5 mm precompression case. All stiffnesses of the precompressed rubber springs were higher than those of the uncompressed one. In particular, the dynamic stiffnesses were higher than those of the quasi-static loading case. The stiffnesses for the second cycles were a little higher than those of the first cycles. Therefore, it was determined that, for the precompressed rubber springs, the loading stiffness becomes higher with more precompression and high loading frequency.

### 3.3.3 Damping effect

The damping ratios for the precompressed rubber springs are shown in Table 2. The average damping ratios of the first and second cycle for the 5 mm precompression case were 3.45% and 2.58%, respectively. The corresponding values for the 10 mm precompression case were 2.1% and 1.63%, respectively. For the non-precompression case, the values were 4.26% and 3.0%. Thus, it is observed that more precompression produced a smaller damping ratio. In addition, the damping ratios for the precompression cases seem to be stable in relation to the loading frequency.

## 4. SMART DAMPER

### 4.1 A new concept of a smart damper

Smart dampers for civil structures should provide sufficient energy dissipation as well as recentering capacity, which are seriously required for the seismic protection of structures. For this purpose, in general, two types of elements are combined; the first one is an element to provide recentering and the other is for damping. Previously, linear elastic and hysteretic damping were combined, but the combination left residual deformation. With increasing damping, the residual deformation increases. To overcome this problem, the damping element should be combined with the rigid-elastic element as shown in Figure 14.

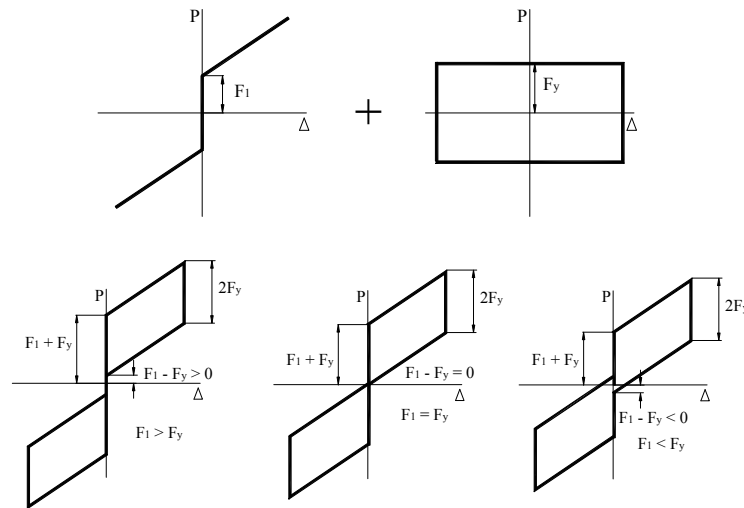


Figure 14 : Smart behavior with combination of rigid elastic behavior and friction

If the rigid force  $F_1$  is greater than the damping force  $F_y$ , the combined behavior returns to the original location with some remaining force; this behavior is called ‘flag-shaped’. The critical rigid force is equal to the damping force. Then, the behavior is restored to the origin with zero force and zero residual deformation. However, the rigid force is smaller than the damping force, and there is residual deformation after unloading. The combination of magnetic friction and a precompressed rubber spring provides the functions of a smart damper, such as recentering capacity and sufficient damping to dissipate energy. A schematic drawing of the smart damper is shown in Figure 15.

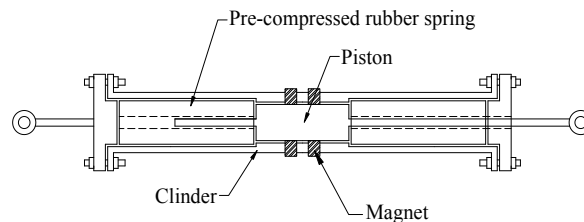


Figure 15 : A smart damper using combination of magnetic friction and precompressed rubber springs

A piston attached by magnets is located at the center, and two rubber springs are placed beside it. The precompression of the two rubber springs is introduced by driving the bolts at the end of the damper; the movement of the springs is blocked by the projecting parts of the cylinder. When the shaft is moving in a direction, friction is generated, and one of the two rubber springs is compressed. When it is moving in the other direction, the other spring is compressed.

#### 4.2. Analytical model of the smart damper

In the precompressed rubber spring, the loading and unloading rigid forces ( $F_2$  and  $F_1$ ) are different. Thus, the unloading rigid force  $F_1$  should be greater than the frictional force  $F_y$ , and then the damper will be placed back at the original location. This combination of a rubber spring and magnetic friction is illustrated in Figure 22. When  $F_1$  is larger than  $F_y$ , the damper returns to the original place with the remaining force of  $F_1 - F_y$ . Nine types of force-combinations are modeled using the OpenSEES program [19], which is generally used for

the seismic nonlinear time-history analyses of civil structures. For the model, two elements are used with parallel combination; the first element is ‘Self-centering’ element for recentering, which shows bilinear and elastic unloading, and the second one is ‘Steel 01’ element for energy dissipation, which shows bilinear plastic behavior. Figure 16 illustrates the behaviors of the elements including the combined behavior of the two elements.

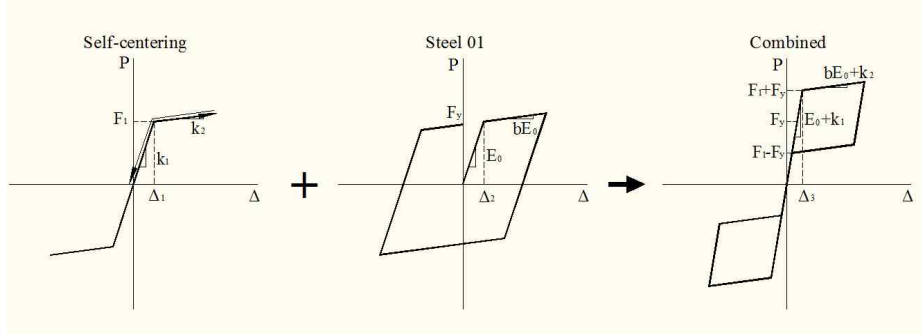


Figure 16 : Combined behavior of precompressed rubber springs and magnetic friction

In the figure,  $E_0$  and  $k_1$  are initial stiffnesses of the two elements, and  $bE_0$  and  $k_2$  are their second stiffnesses, where  $b$  is strain-hardening ratio.  $\Delta_1$  and  $\Delta_2$  are the deformations for initial elastic limit. In the combined behavior, the strength and stiffness depend on those of the two elements. In the models, the frictional force is fixed as 5.0 kN, and the unloading rigid force  $F_1$  varies as 10, 5, and 2.5 kN; the first one is greater than the friction; the second one is equal to the friction; and the third one is less than the friction. The differences  $F$  between  $F_1$  and  $F_2$  have three cases of 5, 2.5, and 0. Table 3 illustrates the combination of the forces.

$F_y$	5								
$F_1$	10 ( $F_1 > F_y$ )			5 ( $F_1 = F_y$ )			2.5 ( $F_1 < F_y$ )		
$\Delta F$	5	2.5	0	5	2.5	0	5	2.5	0
$F_2$ ( $=F_1+\Delta F$ )	15	12.5	10	10	7.5	5	7.5	5.0	2.5

Table 3 : Combination of forces in analytical models of smart dampers

Figure 17 shows hysteretic curves for the nine types of analytical models.

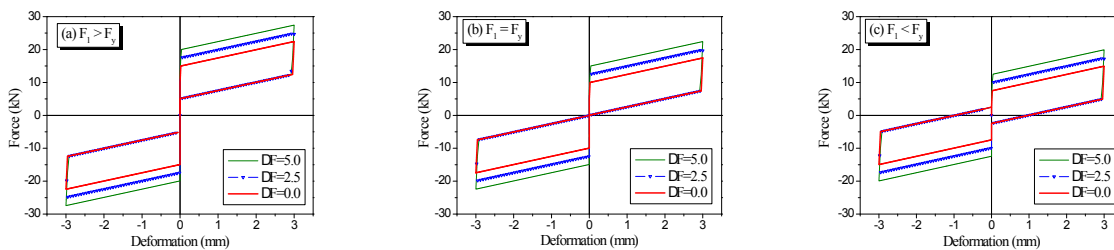


Figure 17 : Analytical models of the smart dampers varying with the rigid forces

It is noticeable that the loading rigid force of the rubber spring does not influence the recentering capacity of the damper. However, if the difference  $F$  is larger, the damping increases. The results also indicate that the recentering capacity is controlled by the unloading rigid force in comparison with the friction

### 4.3. Discussion of application

[10] developed a smart damper that combines martensite and austenite shape memory alloy (SMA) wires. The martensite SMA wires provide energy dissipation, while the austenite SMA wires generate recentering capacity. With this combination, if the low stress plateau of the austenite SMA is higher than the transformation stress of the martensite SMA, the device is recentered without residual deformation after unloading. The concept of the damper proposed in this study is very similar to that of Dolce. However, Dolce's SMA wire damper is relatively expensive since SMA materials are much more expensive than steel and rubber. Thus, the damper with rubber springs and magnets could be manufactured and provided cheaply. If permanent magnets are used, the damper would be a passive type. However, if electronic magnets are used, the damper would be an active type since the magnetic friction can be activated following the clue of vibration in a system. In addition, the electronic current can be controlled according to the magnitude of vibration in a system; in this case, the damper would be adaptive. Therefore, the damper with rubber springs and magnetic friction could be a smart, cheap, and effective option for various applications.

### 5. Conclusion

This study proposed a new concept of a smart damper using precompressed rubber springs and magnetic friction. Dynamic tests of magnetic frictional dampers and precompressed rubber springs were separately conducted. For the tests, permanent magnets having an ultimate adhesive force of 0.8 kN were used. The magnetic friction showed exactly the same behavior as other mechanical frictions; they showed almost perfectly rectangular behavior. The frictional coefficient of the magnets was estimated using an averaging method or linear regression according to the loading frequency. The two methods resulted in similar coefficients, but the regression method seems to be more reliable than the simple averaging method. The frictional coefficient of the magnets increased up to the loading frequency of 0.5 Hz and then became stable. Thus, the dynamic coefficients were larger than the static or pseudostatic coefficient. The overall average frictional coefficient of the magnet was 0.522. In the test of the rubber springs, a cylinder with a hole at the center made of polyurethane rubber was tested. In the test without precompression, the rubber spring showed hysteretic behavior, and the first cycle did not coincide with the subsequent cycles, which showed almost the same path. This was caused by the unrecovered residual deformation of the rubber spring when it was reloaded. The loading paths according to the loading frequency followed the same path except for the case of 0.1 Hz. When the rubber spring was compressed before the test, the spring showed rigid force as expected. The rigid force increased with more precompression in the rubber spring. In these tests, the first cycle was different from the subsequent cycles because of unrecovered residual deformation. The rigid force of unloading was smaller than that of loading; because of the unrecovered residual deformation. Thus, the rubber springs with precompression showed flag-shaped behavior thus provided recentering capacity and damping. The stiffness of the precompressed rubber spring increased with increasing loading frequency for both loading and unloading paths. To embody a smart damper, the magnetic friction and the precompressed rubber springs are combined; in this combination, the magnets provide energy dissipation and the springs provide recentering capacity. For this purpose, the rigid force of unloading should be larger than the frictional force. Then, the damper would return to its initial place without any residual deformation and provide sufficient damping. This concept was proved using analytical models of the OpenSEES program. The rigid force of the loading path increased

damping but did not influence the recentering capacity, which was controlled by the rigid force of the unloading path.

## REFERENCES

- [1] Tubaldi E, Barbato M and Asta AD. Performance-based seismic risk assessment for buildings equipped with linear and nonlinear viscous dampers, *Engineering Structures* 2014; 78:90-99.
- [2] Wang YJ, Yau JD and Wei QC. Vibration suppression of train-induced multiple resonant responses of two-span continuous bridges using VE dampers, *Journal of Marine Science and Technology* 2013; 21(2):149-158.
- [3] Pereira E, Diaz IM, Hudson EJ and Reynolds P. Optimal control-based methodology for active vibration control of pedestrian structures, *Engineering Structures* 2014; 80:153-162.
- [4] Lin YY, Cheng CM and Sun D. Wind-induced vibration control of long span bridges by multiple tuned mass dampers, *Tamkang Journal of Science and Engineering*, 2000; 3(1):1-13.
- [5] Ding Y, Zhang L, Zhu H and Li ZX. A new magnetorheological damper for seismic control, *Smart Materials and Structures*, 2013; 22:115003.
- [6] Yang MG, Li CY and Chen ZQ. A new simple nonlinear hysteretic model for MR damper and verification of seismic response reduction experiment, *Engineering Structures* 2013; 52:434-445.
- [7] Dyke SJ, Spencer BF, Sain MK and Carlson JD. Modeling and control of magnetorheological dampers for seismic response reduction, *Smart Materials and Structures*, 1996; 5:565-75.
- [8] Symans MD and Constantinou MC. Seimi-active control systems for seismic protection of structures: a state-of-the-art review, *Engineering Structures* 1999; 21:469-487.
- [9] Ozbulut OE, and Hurlebaus S. Recentering variable friction device for vibration control of structures subjected to near-field earthquakes, *Mechanical Systems and Signal Processing* 2011; 25:2849-2862.
- [10] Dolce M, Cardone D and Marnetto R. Implementation and testing of passive control devices based on shape memory alloys, *Earthquake Engineering and Structural Dynamics* 2000; 29:945-968.
- [11] Filiatrault A, Tremblay R and Kar R. Performance evaluation of friction spring seismic damper, *Journal of Structural Engineering*, ASCE 2000; 126(4):491-499.
- [12] Christopoulos C and Filiatrault A. Principle of passive supplemental damping and

seismic isolation, IUSS Press 2006, Pavia, Italy.

[13] Bae JS, Kwak MK and Inman DJ. Vibration suppression of a cantilever beam using eddy current damper, *Journal of Sound and Vibration* 2005; 284:805-824.

[14] Sodano HA, Bae JS, Inman DJ and Belvin WK. Concept and model of eddy current damper for vibration suppression of a beam, *Journal of Sound and Vibration* 2005; 288:1177-1196.

[15] Watanabe T, Suzuki K, Iiyama F and Sodeyama H. Experimental study on ball screw type magnetic friction damper: semiactive control using electromagnet, *Journal of Pressure Vessel Technology*, 2004; 126:110-114.

[16] Omata K, Arakawa T and Mezaki Y. Long stroke magnetic damper for a seismic isolation device for machines, 13<sup>th</sup> World Conference on Earthquake Engineering 2004; Paper No. 46.

[17] Oh SW, Choi E and Jung HY. The estimated stiffness of rubber pads for railway bridges, *Journal of Korean Society of Steel Structures* 2005; 17(3):307-316.

[18] Chopra AK. *Dynamics of structures: Theory and Applications to Earthquake Engineering*, 2007, Pearson Prentice Hall.

[19] OpenSEES Development Team. *Open System for Earthquake Engineering Simulation* 2010, Version 2.21, Berkeley, CA, US.